

1 **Directionality and Polarization of Response Spectral** 2 **Ordinates in the 2023 Kahramanmaras, Türkiye Earthquake** 3 **Doublet**

4 **Nathan Girmay,^{a)} M.EERI, Alan Poulos,^{a)} M.EERI, Eduardo Miranda^{a)} M.EERI**

5 Until recently, the orientation of maximum spectral response was generally
6 believed to not have a predominant orientation at rupture distances greater than
7 5 km. However, a recent study found that the orientation of maximum spectral
8 response for strike-slip earthquakes in the NGA-West2 database tends to occur
9 close to the epicentral transverse orientation, that is, an orientation perpendicular
10 to a line connecting the epicenter to the station. This paper investigates
11 directionality in the February 6, 2023, Türkiye doublet earthquakes (M_w 7.8 and
12 7.5) with strike-slip faulting. The orientation of maximum response of 5%-
13 damped linear elastic oscillators was studied. The spatial distribution of the level
14 of polarization, which in this paper refers to the amount of directionality, and
15 intensities at specific orientations were also studied. The maximum spectral
16 response was found to occur systematically close to the epicentral transverse
17 orientation, consistent with previous observations for other strike-slip
18 earthquakes. For the M_w 7.8 event where the location of maximum slip was
19 relatively far from the epicenter, it was found that the orientation of maximum
20 response is, on average, closer to the maximum slip transverse orientation (that
21 is, perpendicular to a line connecting the station to the surface projection of the
22 point of maximum slip) when compared to the epicentral transverse orientation
23 over most period ranges. This suggests that the maximum slip transverse
24 orientation may be a better estimator for determining the orientation of maximum
25 response in large-magnitude strike-slip earthquakes, although further study using
26 more events is warranted. Polarized motions were observed over large
27 geographical areas, and the orientation of maximum response was found to be
28 close to the epicentral or maximum slip transverse for Joyner-Boore distances up
29 to the farthest studied (400 km). These findings further support the case for the

^{a)} Department of Civil and Environmental Engineering, Stanford University, Stanford, CA, USA

30 development of orientation-dependent ground motion models for strike-slip
31 earthquakes.

32 **INTRODUCTION**

33 Earthquake ground motions at a given site are typically recorded in two horizontal and one
34 vertical components. The two horizontal components of ground motion can be combined
35 into a single time series associated with a specific azimuth and rotated incrementally to
36 obtain an intensity in any specified orientation at a given site (Boore, 2010). It is well
37 known that the intensity of horizontal ground motion can vary significantly with changes
38 in orientation, a phenomenon referred to as directionality (Hong and Goda, 2007; Shahi
39 and Baker, 2014; Poulos and Miranda, 2022). Although this variation in intensity with
40 orientation has been known for years, current ground motion models (GMMs) provide
41 estimates of a single scalar measure of ground motion intensity, therefore neglecting
42 directionality effects. Prior studies have proposed different ways of obtaining this scalar
43 measure of ground motion intensity at a given site. For example, Joyner and Boore (1982),
44 Boore et al. (1997), and Abrahamson and Silva (1997) used the geometric mean of
45 intensities of the two as-recorded horizontal intensities. Boore et al. (2006) and Boore
46 (2010) proposed the use of horizontal intensities that are independent of horizontal sensor
47 orientations. Other works have studied ratios between different scalar measures of ground
48 motion intensity at a site (e.g., Beyer and Bommer, 2006; Boore and Kishida, 2017).

49 When studying the effects of rupture directivity, Somerville et al. (1997) observed that for
50 periods longer than 0.6 s, the response spectral ordinates at the strike-normal orientation
51 tended to be larger than those at the strike-parallel orientation, implying that the
52 orientations of maximum intensity are closer to the strike-normal orientation. Follow up
53 studies found that there was indeed a higher probability of the orientation of maximum
54 intensity being closer to the strike-normal orientation but only at rupture distances less than
55 5 km (e.g., Huang et al., 2008; NEHRP Consultants Joint Venture, 2011; Shahi and Baker,
56 2014). For rupture distances greater than 5 km, these other studies observed that the angle
57 between the orientation of maximum intensity and the fault strike did not exhibit a clear
58 pattern, and was essentially random with an approximate uniform probability distribution.
59 Accordingly, current seismic design standards in the United States for conducting response
60 history analysis indicate that sites located away from near-fault regions do not exhibit
61 predominant orientations (ASCE, 2016; 2022).

62 The studies mentioned in the previous paragraph focused on studying directionality of
63 spectral response with respect to the fault strike (i.e., strike-normal or strike-parallel), that
64 is, with respect to an orientation common to all recording stations. In a contrasting
65 approach, Poulos and Miranda (2023) studied the orientation of maximum spectral
66 response with respect to the epicentral transverse orientation, which is the orientation
67 perpendicular to a line segment connecting the station to the epicenter. This orientation, in
68 general, is different for each recording station and is defined by the position of each station
69 relative to the epicenter. They used the NGA-West2 ground motion database (Ancheta et
70 al., 2014) to investigate the orientation of maximum response of 1966 ground motions
71 recorded on strike-slip earthquakes and 2226 ground motions recorded on reverse-faulting
72 earthquakes that had moment magnitudes greater than or equal to five. They found that for
73 strike-slip events, there was a notable tendency for the orientation of maximum spectral
74 response to be close to the transverse orientation. Additionally, they concluded that the
75 orientation of maximum intensity got closer to the transverse orientation as oscillator
76 period increased. This finding is significant since it means that the probability distribution
77 of the orientation of maximum intensity is not uniform as previously thought and that it
78 can be estimated from the geographic location of the site relative to the location of the
79 epicenter.

80 Poulos and Miranda's (2023) motivation for examining the orientation of maximum
81 response with respect to the transverse orientation was that S waves from theoretical double
82 couple point sources in a homogenous medium exhibit polarization transverse to the
83 direction of propagation. In their study, they used the epicenter as the location of the point
84 source. However, ground motion at a specific location is caused by a combination of
85 waveforms produced by slip occurring at different points on the fault rupture. Given that
86 the location of maximum slip is the principal contributor to the total slip that generated the
87 earthquake, it may be a better point source for the radiation patterns. For smaller magnitude
88 earthquakes, the location of maximum slip may be located close to the epicenter.
89 Conversely, for large-magnitude events, it is not uncommon for the location of maximum
90 slip to be far from the epicenter. For example, using more than 80 finite-source rupture
91 models for 50 earthquakes, Mai et al. (2005) found that rupture initiates in regions of low
92 slips in 48% of the events they investigated. The hypocenter occurred in regions of very
93 large slips in only 15% of the events. Therefore, there may be limitations to using the

94 epicenter to estimate orientations of maximum spectral response for large-magnitude
95 events.

96 The February 6th, 2023 Kahramanmaras earthquake doublet generated one of the most
97 extensive collections of strong motion data recorded to date from strike-slip events with
98 moment magnitudes above 7.4. Hence, this earthquake doublet provides an exceptional
99 opportunity to validate and further study the observations by Poulos and Miranda (2023)
100 for strike-slip earthquakes. The epicenter for the larger magnitude mainshock was located
101 relatively far from points of large slip and thus also provides an opportunity to investigate
102 how well the epicentral transverse works in predicting orientation of maximum response.

103 This work studies the directionality of ground motions recorded during the 2023
104 Kahramanmaras earthquake sequence, focusing on the M_w 7.8 and M_w 7.5 doublet. The
105 orientation of maximum intensity for 5%-damped linear elastic oscillators subjected to the
106 ground motions as well as their spatial distribution is investigated. The work of Poulos and
107 Miranda (2023) is extended by investigating the orientation of maximum response with
108 respect to the transverse orientation of a line segment connecting a station and the surface
109 projection of the point of maximum slip. That is, the point of maximum slip is treated as
110 the point source for radiation patterns and its ability to predict the orientation of maximum
111 intensity for the Türkiye doublet is investigated. A comparison between using maximum
112 slip transverse and epicentral transverse is provided. The spatial distribution of
113 polarization, which in this paper refers to the *amount* of directionality quantified by the
114 ratio between the minimum and maximum spectral response within the horizontal plane,
115 and intensities at transverse and radial orientations are also evaluated. Additionally, the
116 possible influence of the level of polarization on the angular difference between the
117 orientation of maximum intensity and epicentral transverse orientation is studied.

118 **SELECTION OF EARTHQUAKE GROUND MOTION RECORDS**

119 The Türkiye sequence initiated on February 6, 2023, at 01:17 (UTC) with the M_w 7.8
120 earthquake on a north-east-striking fault previously mapped as the Sakçagöz and Narlı
121 segments of the Dead Sea fault (DSF) (Emre et al., 2018) and propagated to the Erkenek,
122 Pazarcık and Amanos segments of the East Anatolian Fault (EAF) in southern Türkiye. The
123 epicenter for this first event occurred at 37.226°N, 37.014°E near the town of Şatırhüyük,
124 in the Nurdağı district of the Gaziantep province, with a focal depth of 10 km (USGS,

125 2023a). USGS focal mechanism solutions found the event, henceforth called the M_w 7.8
126 Kahramanmaras earthquake, occurred due to strike-slip faulting on a nodal plane with a
127 strike of 228° , a rake of -1° , and a dip of 89° . The M_w 7.5 event occurred approximately
128 nine hours after the first event at 10:24 (UTC) on the Sürgü and Çardak faults which are
129 splay faults of the EAF with an epicenter located northeast of Kahramanmaras at 38.011°N ,
130 37.196°E . The focal depth for the event, henceforth called M_w 7.5 Elibistan earthquake,
131 was 7.4 km and the faulting style was strike-slip occurring on a nodal plane with a strike
132 of 277° , a rake of 4° , and a dip of 78° (USGS, 2023b). Following the two major events,
133 numerous aftershocks were recorded, with over 400 of the aftershocks having moment
134 magnitudes greater than five (EERI and GEER, 2023). This paper focuses only on the M_w
135 7.8 and 7.5 events.

136 The strong motion network operated by AFAD consists of the Turkish National Seismic
137 Network (TNSN) and the Turkish National Strong Motion Network (TNSMN), initially
138 installed with analog instruments in 1973 and updated over time to include over 327
139 stations with digital instruments by 2009 (Akkar et al., 2009). The considerable extent of
140 shaking and the wide adoption of seismic instrumentation in Türkiye makes this doublet
141 two of the best recorded strike-slip events with moment magnitudes above 7.4. Soon
142 following the events, AFAD released the strong motions recorded in both networks. This
143 paper uses the processed versions of these ground motion records. The record processing
144 performed by AFAD followed the procedure proposed by Paolucci et al. (2011) which
145 includes mean removal, baseline correction, instrument correction, and band-pass filtering
146 using a second order acausal frequency-domain Butterworth filter.

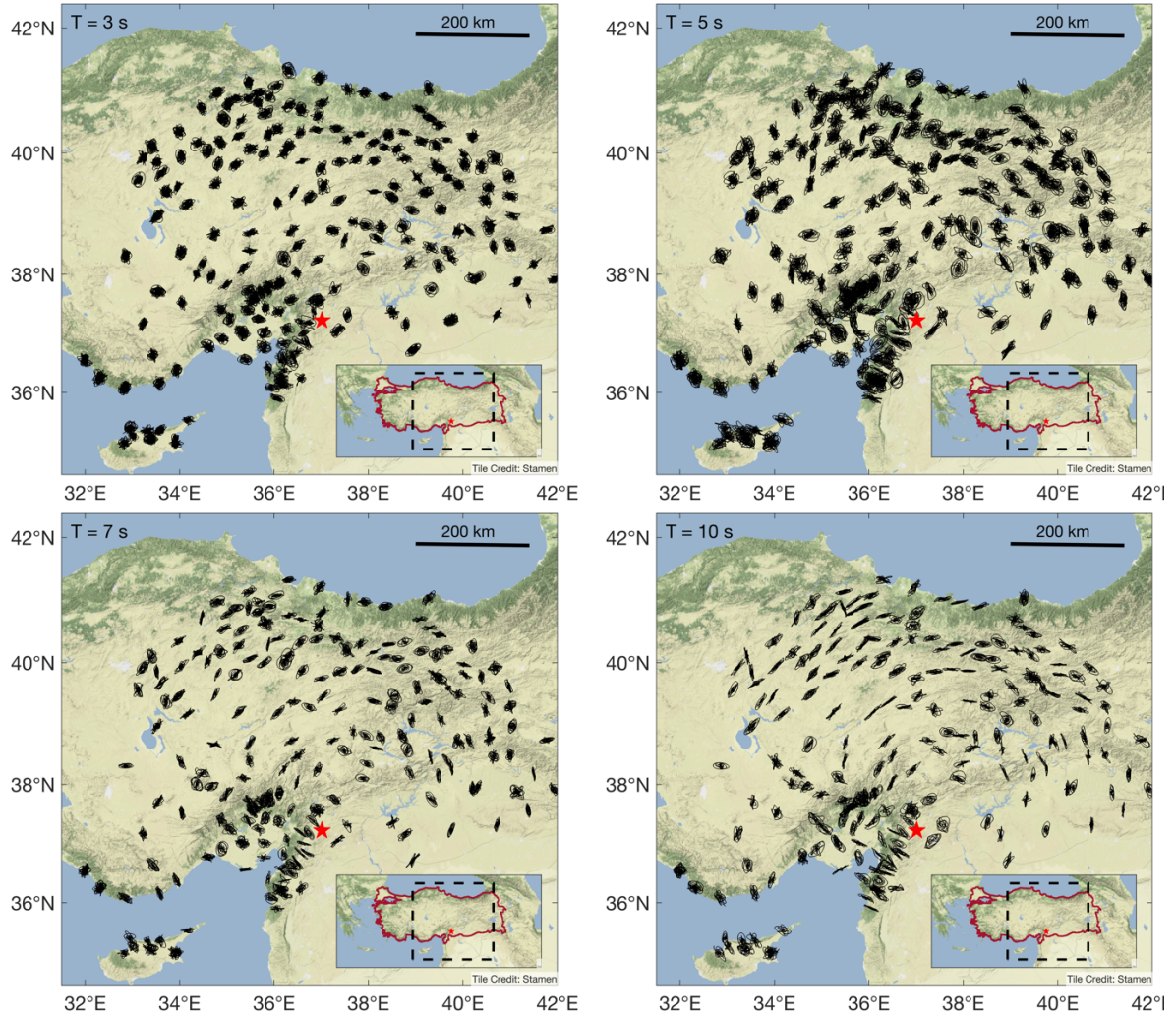
147 The strong motion records used in this study were selected based on the following criteria.
148 Firstly, since the study of directionality requires both horizontal components and their
149 orientations, only stations that recorded both horizontal components, and where the
150 azimuths of each component are known were considered. Secondly, only records where at
151 least one of the two as-recorded horizontal components had a peak ground velocity (PGV)
152 of 1 cm/s were considered. This criterion guarantees a strong signal-to-noise ratio for a
153 wide range of periods, especially for the long-period range. Lastly, for records that passed
154 the requirements above, the oscillator response was evaluated only up to the maximum
155 usable period for the record (Boore, 2004), which was calculated as 1 divided by 1.25 times
156 the low-pass corner frequency following the method of Abrahamson and Silva (1997). This

157 last criterion is necessary to ensure that the signals used for long-period oscillators are
158 suitable. The available records were then visually evaluated to identify and remove
159 waveforms that had recording issues such as early termination or late start. Overall, a total
160 of 231 records for the M_w 7.8 event and 222 records for the M_w 7.6 event passed the filtering
161 criteria outlined above.

162 **ORIENTATION OF MAXIMUM INTENSITY**

163 The most commonly used measure of ground motion intensity in earthquake engineering
164 is the 5%-damped response spectral ordinate, which represents the peak response of a
165 single-degree-of-freedom linear elastic oscillator with a damping ratio of 5% at different
166 periods of vibration. The bidirectional response of a given oscillator can be computed when
167 subjected to the two horizontal components recorded at a specific station, and the
168 oscillator's movement can be tracked to generate a vectorial trace of the response in the
169 horizontal plane or hodograph. Figure 1 shows the spatial distribution of the recording
170 stations considered for the M_w 7.8 Kahramanmaras earthquake and the relative
171 displacement hodograph of 5%-damped oscillators for four different natural periods when
172 subjected to the horizontal components of ground motions recorded at each station. See
173 Figure ES2 in the electronic supplement for a similar figure but for the M_w 7.5 Elbistan
174 earthquake. In these figures, each hodograph is normalized by the maximum spectral
175 response at each station such that the normalized peak amplitude is the same for all stations.
176 In general, the displacement traces shown in the figure have an approximately elliptical
177 shape with major axes clearly larger than the minor axis, suggesting that the oscillator
178 response tends to have a preferred orientation of larger intensity. It is apparent that across
179 the four periods shown, the hodographs for stations that are in close geographic proximity
180 to each other generally have similar displacement traces. These findings are consistent with
181 the recent observations made by Poulos and Miranda (2023). Additionally, it is apparent
182 that the orientation of response in the hodographs of adjacent stations becomes even more
183 similar as the period of oscillation increases.

184



185 **Figure 1.** Spatial distribution of relative displacement hodographs of 5% damped linear elastic
 186 oscillators subjected to ground motions recorded during the 2023 M_w 7.8 Kahramanmaraş
 187 earthquake. Oscillator period is shown in the top left corner of each panel. The hodographs are
 188 normalized to fit inside a circle with a radius equal to the maximum recorded displacement.

189 The maximum spectral response at each recording station shown in Figure 1 corresponds
 190 to the point in the relative displacement history that is farthest from the resting point
 191 (origin) in each hodograph. For an oscillator with a given natural period and a relative
 192 displacement response history $u_x(t)$ and $u_y(t)$ in two perpendicular horizontal
 193 components, the maximum response (also known as RotD100) in all orientations is
 194 computed as

195
$$\text{RotD100} = \max_t \sqrt{u_x(t)^2 + u_y(t)^2} \quad (1)$$

196 As such, the orientation of maximum response corresponds to the orientation of this point
 197 farthest from the origin of each hodograph, defined as follows

198
$$\phi_{RotD100} = atan2[u_y(t_{@max}), u_x(t_{@max})] \quad (2)$$

199 where $atan2(y, x)$ is the four-quadrant inverse tangent and $t_{@max}$ is the time at which
 200 RotD100 occurs.

201 Alternatively, the maximum response can also be determined by first combining the two
 202 recorded horizontal responses into a single time series, $u(t, \phi)$, associated with an azimuth
 203 (as defined from true north) and then incrementally rotating over 180° as follows

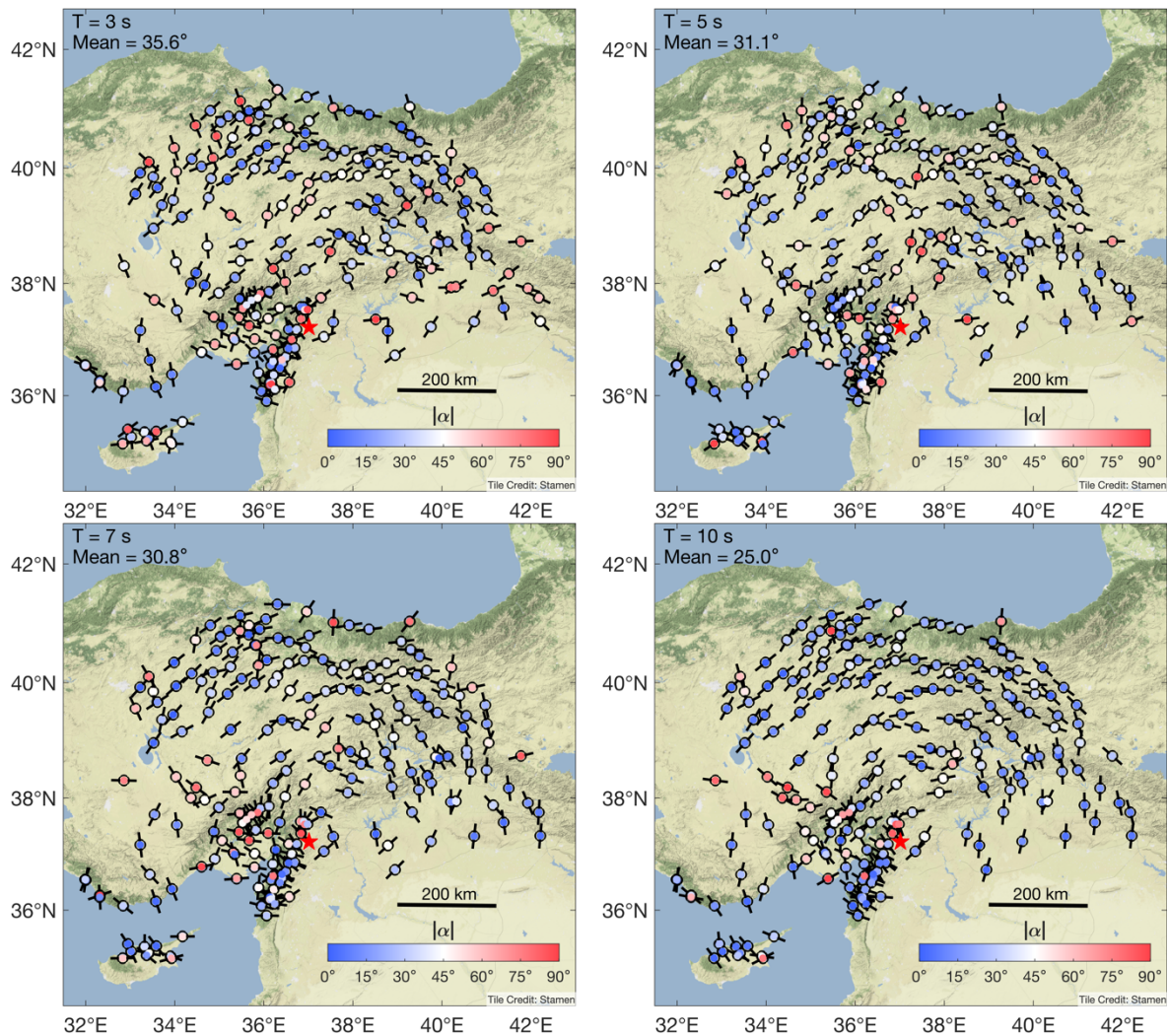
204
$$u(t, \phi) = u_x(t) \cos(\phi) + u_y(t) \sin(\phi) \quad (3)$$

205
$$RotD100 = \max_{t, \phi} |u(t, \phi)| \quad (4)$$

206 However, calculation with Equations (1) and (2) is significantly faster than with (3) and
 207 (4). The orientation of maximum response is the azimuth associated with the maximum
 208 intensity within the rotations (Boore, 2010).

209 Poulos and Miranda (2023) defined the angular difference between the transverse
 210 orientation (i.e., the orientation that is perpendicular to a line segment connecting the
 211 station to the epicenter) and the orientation of maximum intensity as the angle $\alpha \in [-90^\circ,$
 212 $90^\circ]$. This angle is measured with respect to the transverse orientation and is positive if the
 213 orientation of maximum intensity is counterclockwise and negative if clockwise. For this
 214 study, the direction of maximum intensity within the transverse orientation (clockwise or
 215 counterclockwise) is not important. Instead, the absolute angular difference, $|\alpha|$, between
 216 0° and 90° is used. In Figure 2, the colors of the circles at each station indicate the absolute
 217 angular difference for the oscillators subjected to the M_w 7.8 event, with blue circles
 218 indicating the orientation of maximum response is closer to the transverse orientation and
 219 red circles indicating that the maximum response is closer to the radial orientation.

220 Two main observations can be made from Figure 2. First, the orientation of maximum
 221 intensity, as indicated by the short black lines at each recording station, are similar for
 222 stations that are close to each other and over the geographic region appear to form a circular
 223 pattern around the epicenter. Secondly, most stations have blue colored circles, suggesting
 224 that the predominant orientation of maximum intensity appears to be close to the transverse
 225 orientation. Both observations become more apparent as the oscillator period increases. See
 226 Figure ES3 in the electronic supplement for a similar figure for the M_w 7.5 Elbistan
 227 earthquake.

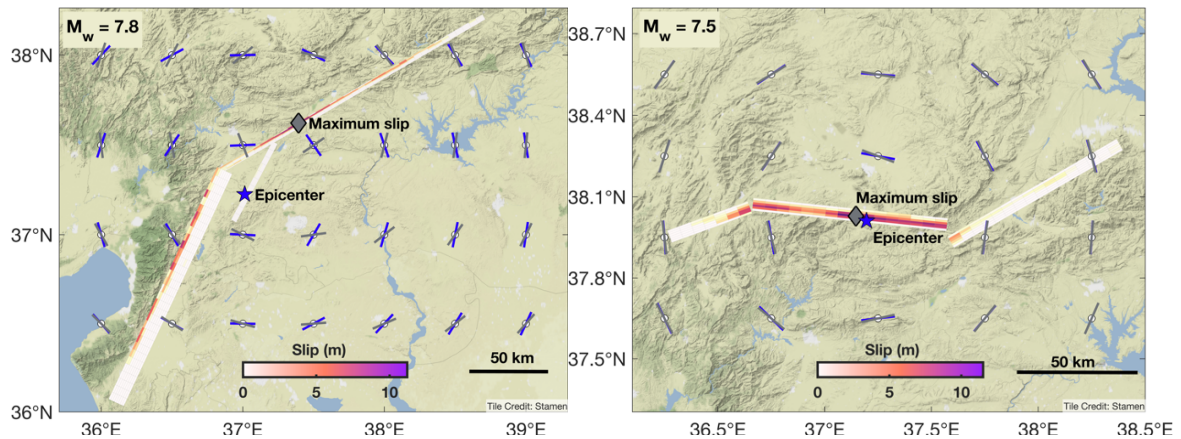


228 **Figure 2.** Orientation of maximum response of 5% damped linear elastic oscillators subjected to
 229 recorded ground motions from the 2023 M_w 7.8 Kahramanmaras Earthquake and their angular
 230 difference with respect to the transverse orientation. The orientation of the maximum response at
 231 each station is shown by short black lines and the angular difference is indicated by the color inside
 232 each circle. Oscillator period and mean $|\alpha|$ for each panel are shown in the top left corner.

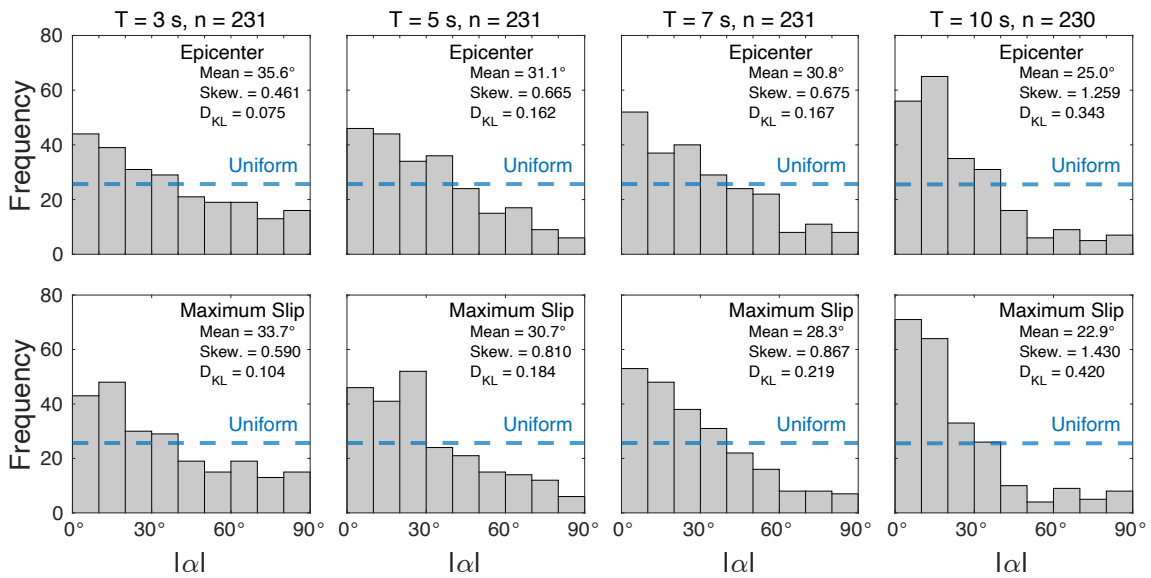
233 As discussed in the introduction, Poulos and Miranda (2023) considered the epicenter to
 234 compute transverse orientations. However, ground displacements at a particular site are the
 235 result of the superposition of various waves generated by slip that occurs at different points
 236 on the rupture surface. Although the maximum slip location may be situated near the
 237 epicenter for smaller magnitude earthquakes, for large magnitude events, it is not
 238 uncommon for the maximum slip location to be far away from the epicenter. Figure 3
 239 shows the horizontal projection of the USGS finite fault models developed for the M_w 7.8
 240 Kahramanmaras and M_w 7.5 Elbistan earthquakes (USGS, 2023a, 2023b). For the larger
 241 magnitude event, it is apparent that the location of maximum slip occurred far from

242 the epicenter (an approximate separation of 55.4 km), whilst for the Elbistan event, the
 243 locations practically coincide (an approximate separation of 4.8 km). For each rupture in
 244 Figure 3, a grid of hypothetical recording stations is included to show that the epicentral
 245 transverse orientation (shown by the blue lines) and the maximum slip transverse
 246 orientation (shown by the grey lines) are notably different in the near field for the case
 247 where the epicenter is located far from the point of maximum slip as it occurred in the M_w
 248 7.8 main event, whereas the two orientations essentially coincide for the M_w 7.5 event.

249 Since the location of maximum slip is the primary contributor to the total slip that generated
 250 the earthquake, it may be a better center/source for the radiation patterns. To examine this,
 251 the absolute angular difference between the orientation of maximum intensity and the
 252 maximum slip transverse orientation (i.e., perpendicular to a line segment connecting the
 253 station and the horizontal surface projection of the point of maximum slip) was computed
 254 for each station. This was then compared to $|\alpha|$ computed using the epicenter as done by
 255 Poulos and Miranda (2023). Figure 4 shows histograms of the angular difference between
 256 the orientation of maximum intensity and the epicentral or maximum slip transverse
 257 orientation for four different oscillators subjected to the M_w 7.8 Kahramanmaras
 258 earthquake. The oscillator periods used in these histograms are the same as those used for
 259 Figures 1 and 2.



260 **Figure 3.** Horizontal surface projection of finite fault models for the (a) M_w 7.8 and (b) M_w 7.5
 261 events per USGS (2023a and 2023b). The epicenter is indicated by the blue star and the location of
 262 maximum slip is indicated by the grey diamond. The epicentral transverse orientation at points
 263 surrounding the fault are shown by the short blue lines, while the maximum slip transverse
 264 orientation is shown by the short grey lines.



265

266

267

268

269

270

Figure 4. Histograms of the angular difference between the orientation of RotD100 and the transverse orientation for oscillators subjected to ground motions recorded during the 2023 M_w 7.8 Kahramanmaras earthquake with periods of $T = 3$ s, $T = 5$ s, $T = 7$ s, and $T = 10$ s. The dashed lines represent the histogram should the orientation of RotD100 be uniformly distributed with respect to the transverse orientation.

271

272

273

274

275

276

277

278

279

280

281

282

283

284

285

From Figure 4 it can be observed that, regardless of whether the epicentral transverse or the maximum slip transverse orientation is considered, the histograms are heavily skewed to small values of $|\alpha|$ and have, in all cases, mean angular differences notably below 45° . Should the orientation of maximum spectral response be equally likely with respect to either the epicentral or maximum slip transverse orientation, the distribution would be more uniform, as indicated by the dashed blue lines, and would have a mean closer to 45° . Inset in each histogram is the Kullback-Leibler divergence (D_{KL}) (Kullback and Leibler, 1951), which in this case measures how much the observed distribution of the histogram differs from a uniform distribution. For reference, a theoretical triangular distribution with maximum density at 0° and zero density at 90° would have a D_{KL} value of 0.1931 relative to a uniform distribution. Should the empirical distributions be perfectly uniform, the D_{KL} value would be zero. However, the D_{KL} values provided on each histogram indicate that the empirical distributions are notably different from a uniform distribution and the maximum intensity tends to occur closer to the transverse orientation. See Figure ES4 in the electronic supplement for a similar figure for the M_w 7.5 Elbistan earthquake.

286

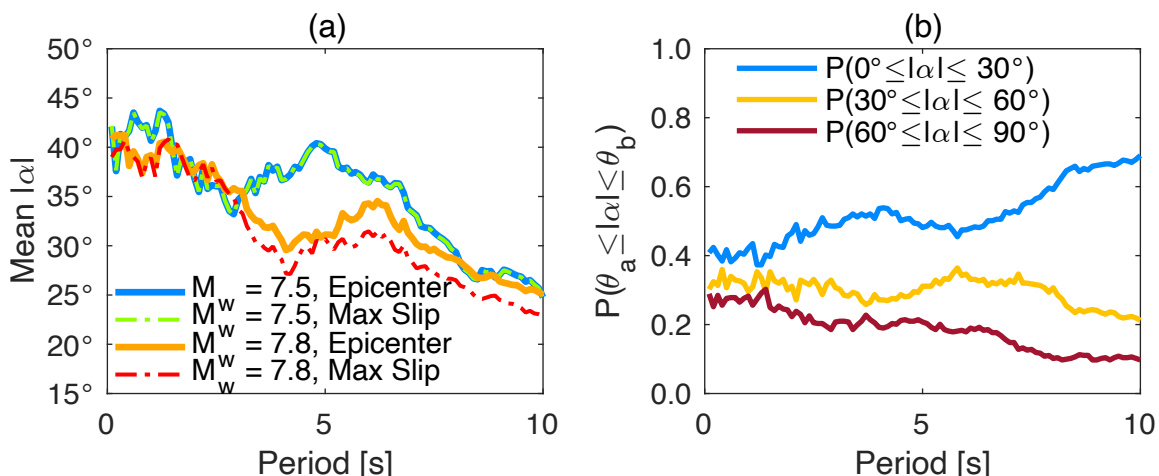
287

288

289

The second significant observation from Figure 4 is that mean $|\alpha|$ tend to be smaller when using the location of maximum slip as the point source than when using the epicenter. Furthermore, for the four periods, using the point of maximum slip to compute the transverse orientations leads to larger skewness coefficients, again indicating that this is a

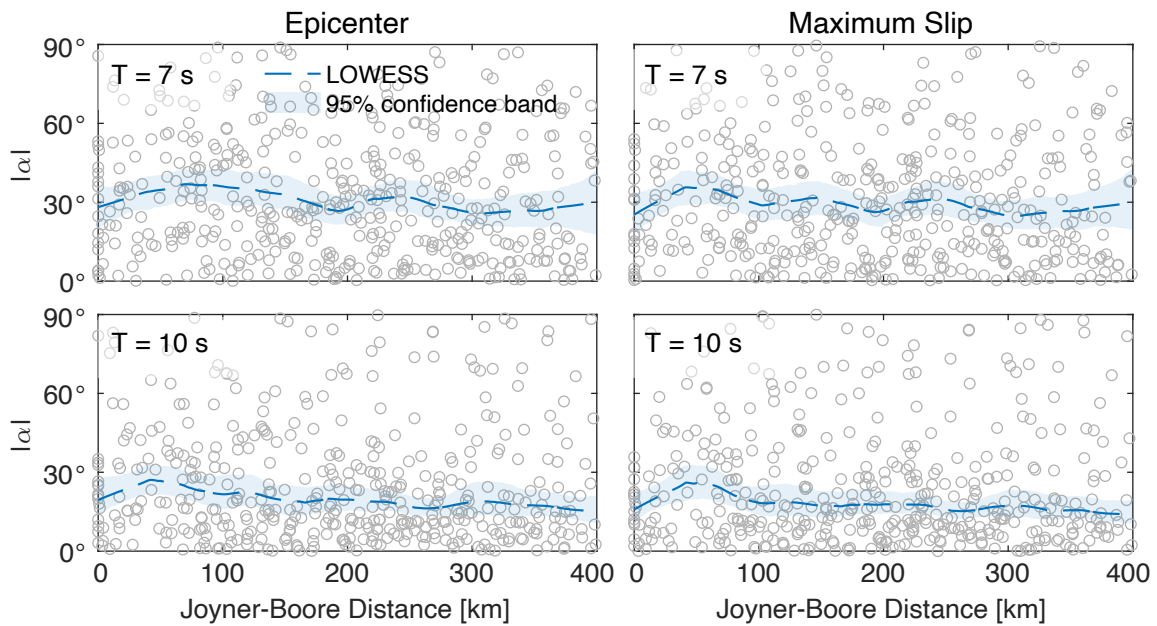
290 better point source for estimating the orientation of maximum response. To better
 291 understand the influence of period on the orientation of maximum response, Figure 5(a)
 292 shows the variation of mean $|\alpha|$ with oscillator period.



293
 294 **Figure 5.** (a) Influence of oscillator’s period of vibration on the mean angular distance between the
 295 orientation of RotD100 and the transverse orientation for oscillators subjected to recorded ground
 296 motions from the 2023 Kahramanmaraş earthquake doublet. The solid lines represent the mean
 297 angular difference computed with respect to the epicentral transverse orientation whilst the dash-
 298 dot lines represent the mean angular difference computed with respect to the transverse orientation
 299 of the point of maximum slip. (b) Probability of the angular difference between the orientation of
 300 RotD100 and the epicentral transverse orientation being between $[0^\circ, 30^\circ]$, $[30^\circ, 60^\circ]$ $[60^\circ, 90^\circ]$.

301 Figure 5(a) confirms that the mean orientation of maximum intensity is, with exception of
 302 a narrow range of periods, closer to the maximum slip transverse orientation for the M_w 7.8
 303 event where the location of maximum slip is far from the epicenter. In contrast, there is
 304 almost no difference in mean $|\alpha|$ for the M_w 7.5 event where the location of the epicenter
 305 and maximum slip practically coincide. This suggests that for these earthquakes the
 306 orientation transverse of the maximum slip is better than the epicentral transverse at
 307 estimating the orientation of maximum intensity, and is likely to be the case for other large-
 308 magnitude strike-slip earthquakes. Additionally, Figure 5(a) shows that mean $|\alpha|$ tends to
 309 decrease with increasing period, meaning that the orientation of maximum intensity gets
 310 closer to the epicentral or maximum slip transverse orientation with increasing period. This
 311 is further illustrated by Figure 5(b), where the probability of being within 30° of the
 312 epicentral transverse shows a tendency to increase with period. For the Türkiye doublet,
 313 the probability that the orientation of maximum spectral response is within 30° of the
 314 epicentral transverse was two to six times higher than the probability of being within 30°
 315 of the radial orientation.

316 Although Poulos and Miranda (2023) investigated the orientation of maximum intensity
 317 with respect to the epicentral transverse, they did not evaluate the influence of source-to-
 318 site distance on $|\alpha|$. Figure 6 evaluates the possible influence of Joyner-Boore distance on
 319 $|\alpha|$ for oscillators subjected to both the M_w 7.8 and 7.5 events. Also shown in each of the
 320 scatter plots is the change in angular difference with increasing distance to the rupture using
 321 locally weighted scatterplot smoothing (LOWESS) and its corresponding 95% confidence
 322 band computed using bootstrapping. Figure 6 suggests that the distance to the source does
 323 not have a notable influence on the orientation of maximum intensity with respect to either
 324 the epicentral or maximum slip transverse for the Türkiye earthquake doublet. The
 325 orientations of maximum spectral response remain closer to the epicentral and/or maximum
 326 slip transverse orientations than a uniform distribution case (as demonstrated by mean $|\alpha|$
 327 values notably below 45°) for all Joyner-Boore distances, indicating that there is a
 328 predominant orientation of maximum spectral response at distances greater than 5 km and
 329 this continues to be the case even for distances as far as 400 km.



330

331 **Figure 6.** Evaluation of the possible influence of Joyner-Boore distance on the angular distance
 332 between the epicentral transverse orientation and the orientation of RotD100 for oscillators with
 333 periods of $T = 7$ s and $T = 10$ s. The dashed line represents locally weighted scatterplot smoothing
 334 (LOWESS) and the shaded area represents 95% confidence bands. These results consider both the
 335 M_w 7.5 and 7.8 events (total of 453 records at 7 s and 452 records at 10 s).

336

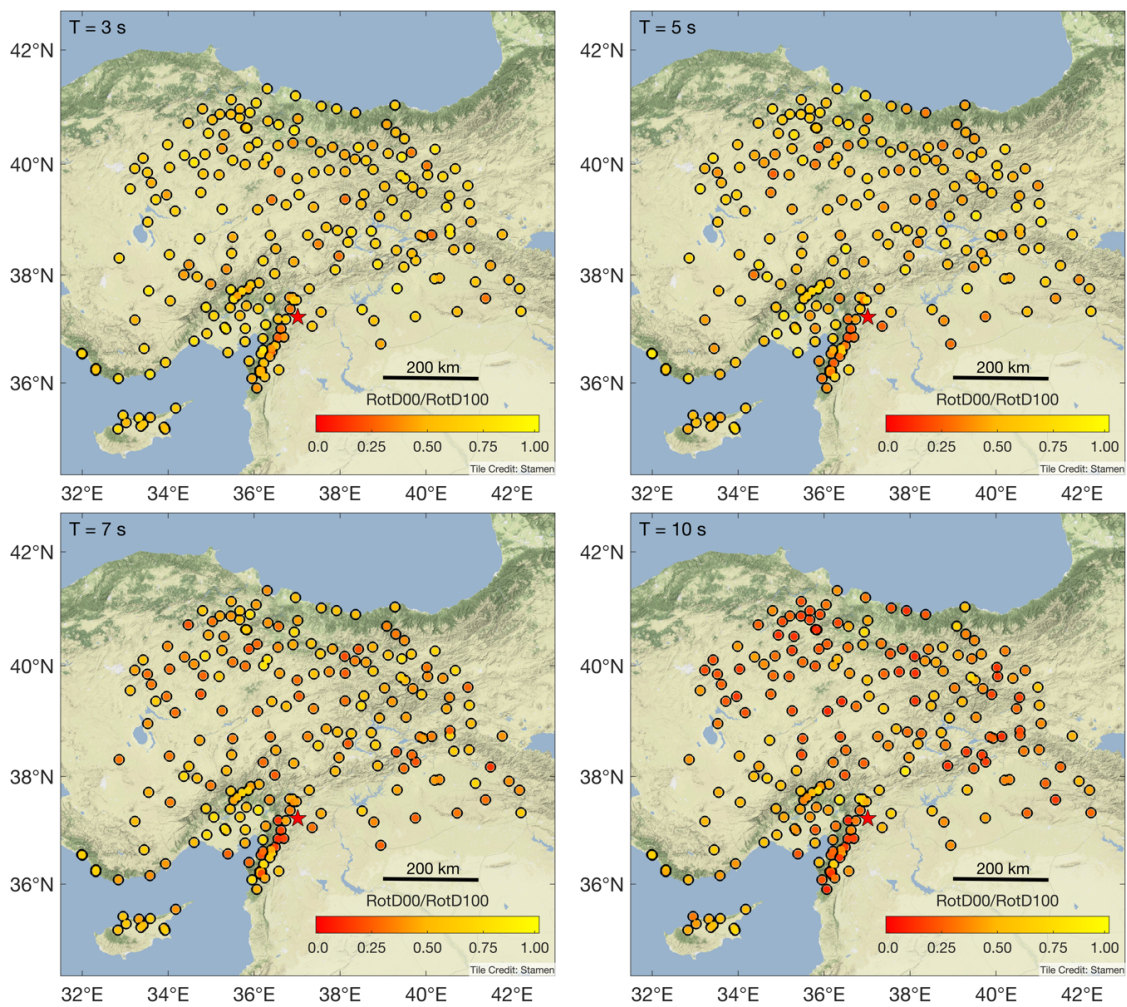
337 **SPATIAL DISTRIBUTION OF POLARIZATION IN RECORDED GROUND**
338 **MOTIONS**

339 As discussed in the prior section, the observed hodographs in Figure 1 tend to have
340 bidirectional responses characterized by elongated elliptical shapes. An oscillator's
341 response is said to be polarized if it exhibits a notably larger intensity in certain orientations
342 than in others. The level of polarization can be qualitatively seen in the shape of the
343 hodographs at each station. However, since there are numerous stations and oscillator
344 periods considered, a quantitative measure of polarization is preferred so that trends can be
345 investigated. In previous studies, the most common method of quantifying the level of
346 polarization has been computing ratios between two scalar intensities for a given station.
347 For example, Shahi and Baker (2014) quantified the level of polarization through the ratio
348 of maximum spectral response (RotD100) and the median spectral response of all
349 orientations (RotD50). An unpolarized ground motion would have RotD100/RotD50 ratio
350 close to 1 whereas a fully polarized motion would have a ratio of $\sqrt{2}$. Whilst this
351 RotD100/RotD50 ratio provides a conversion factor of the median intensity used in GMMs
352 to the maximum intensity used by some design codes (e.g., ASCE, 2022), it does not
353 provide a full measure of polarization in the record as it does not provide information of
354 how much lower the intensity could be in certain orientations.

355 Another method of quantifying the level of polarization is by using the $\eta(90^\circ)$ parameter
356 proposed by Hong and Goda (2007). This parameter represents the ratio of intensity at the
357 major response axis (i.e., RotD100) with respect to the intensity in the perpendicular
358 direction. The ratio is bound between 0 for a fully polarized ground motion and 1 for an
359 unpolarized ground motion. A similar but better measure of the level of polarization of
360 horizontal ground motion is the ratio of the zeroth percentile response (RotD00) and
361 RotD100. This ratio quantifies the *total* variation of the intensity with orientation by
362 providing the ratio of the minimum to maximum intensity experienced by an oscillator
363 when subjected to a ground motion. This ratio is also bound between 0 and 1 with highly
364 polarized motions having values closer to 0 and unpolarized motions having values closer
365 to 1.

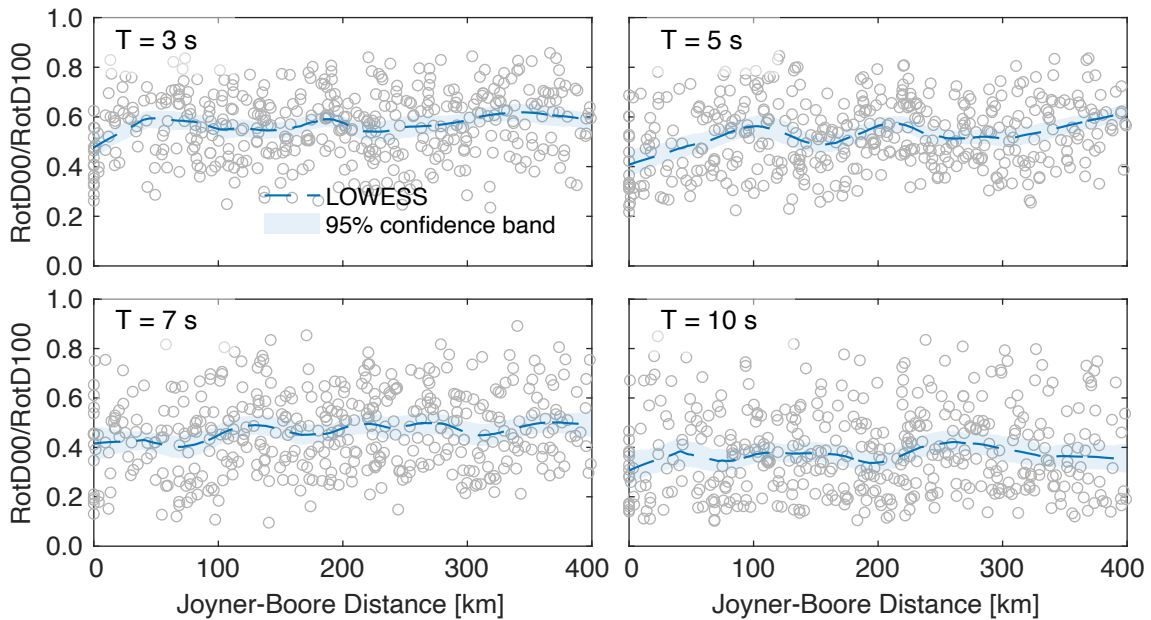
366 Figure 7 shows the spatial distribution of the level of polarization as measured by
367 RotD00/RotD100 for 5% damped oscillators with four different fundamental periods when
368 subjected to ground motions recorded during the M_w 7.8 Kahramanmaras earthquake. The

369 level of polarization is indicated by the color inside the circle located at each recording
 370 station. Stations with low RotD00/RotD100 ratios (i.e., strongly polarized records) are
 371 indicated by red circles, and stations with high RotD00/RotD100 ratios (i.e., records that
 372 are not strongly polarized) are indicated by yellow circles. It can be observed that as the
 373 oscillator period increases, the level of polarization increases. For 10 s oscillators, most
 374 stations are red-orange colored, indicating they are strongly polarized. Furthermore, many
 375 stations that are far from the epicenter and/or rupture are orange/red colored, implying that
 376 even stations far away from the rupture can exhibit strong levels of polarization. Even at 3
 377 s, a large percentage of the stations far from the rupture are orange-colored, and hence fairly
 378 polarized. Similar results were obtained for the M_w 7.5 Elbistan earthquake, which are
 379 available in Figure ES5 of the electronic supplement.



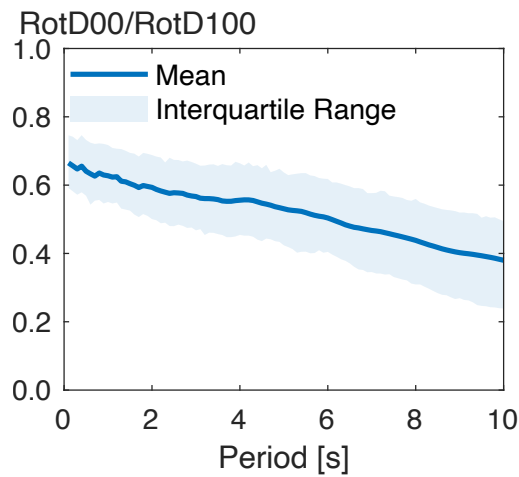
380 **Figure 7.** Geographic distribution of RotD00/RotD100, for 5% damped linear elastic oscillators
 381 subjected to recorded ground motions from the 2023 M_w 7.8 Kahramanmaras earthquake for $T = 3$
 382 s, $T = 5$ s, $T = 7$ s, and $T = 10$ s. A fully polarized motion would be represented by a bright red
 383 circle, and a fully unpolarized motion would be shown by a bright yellow circle.

384 The influence of distance on the level of polarization for the Türkiye doublet is further
 385 examined in Figure 8, which shows RotD00/RotD100 ratios as a function of distance to the
 386 source as measured by Joyner-Boore distance. In this figure, each point on the graph
 387 represents a recording station and the dashed blue line shows a LOWESS with a 95%
 388 confidence band. From this figure, it can be seen that, with the exception of sites less than
 389 25 km from the rupture where the level of polarization decreases with increasing distance,
 390 the level of polarization, in general, remains relatively constant even at very long distances
 391 (e.g. 400 km). It is important to note that even at 400 km, the mean RotD00/RotD100 at 10
 392 s is approximately equal to 0.4, which is still significantly polarized. Figure 8 also shows
 393 that as the oscillator period increases, the scattered points tend to move downwards,
 394 indicating an increase in the level of polarization. This is further emphasized by Figure 9,
 395 which shows that the mean level of polarization increases almost linearly with period. The
 396 interquartile range for the observations, represented by the shaded bands in Figure 9, shows
 397 that although there is some variability in the level of polarization, it is generally not very
 398 large.



399
 400 **Figure 8.** Influence of Joyner-Boore distance on the level of polarization, as measured by
 401 RotD00/RotD100, for 5% damped linear elastic oscillators with periods of 3 s, 5 s, 7 s, and 10 s.
 402 The dashed line represents locally weighted scatterplot smoothing (LOWESS) considering both the
 403 M_w 7.5 and 7.8 events (total of 453 records at 7 s and 452 records at 10 s).

404



405

406 **Figure 9.** Influence of period of vibration on level of polarization, as measured by the mean ratio
 407 of RotD00/RotD100, for 5% damped linear elastic oscillators. Shaded bands around the means
 408 represent the interquartile range of this ratio at each period.

409 So far, it has been illustrated that recorded ground motions in the Türkiye doublet are
 410 polarized even at short periods and tend to become more polarized with increasing period.

411 It has also been shown in the previous section that the orientation of maximum spectral
 412 response appears to be close to the epicentral or maximum slip transverse orientation.

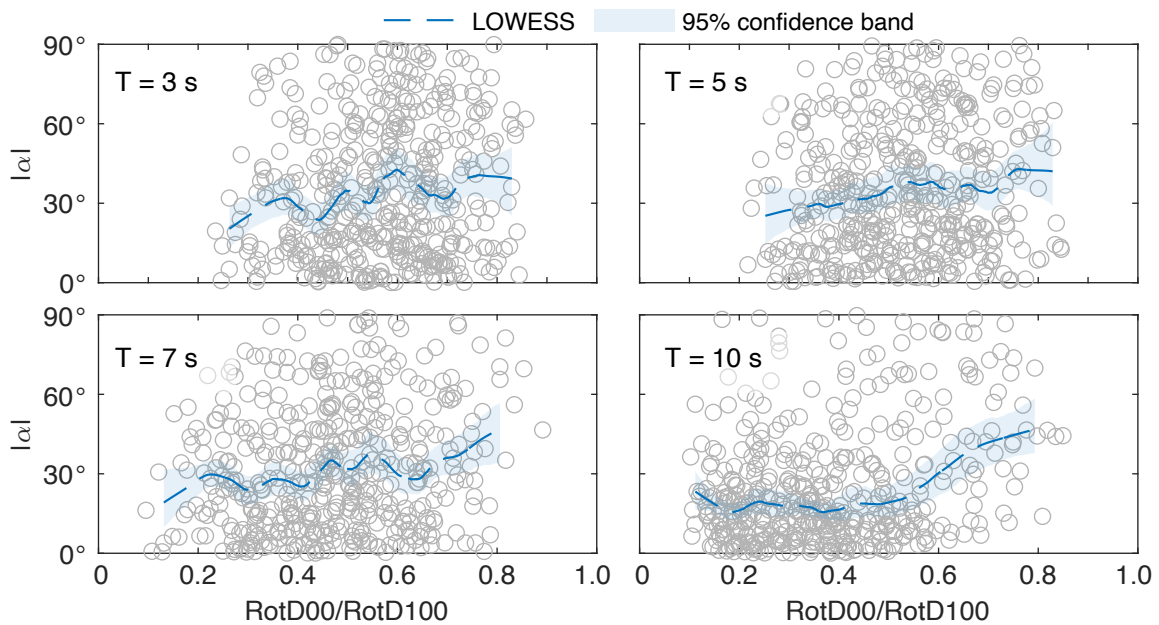
413 Combining both observations, it would be of interest to determine whether the level of
 414 polarization is correlated with the orientation of maximum intensity. Figure 10 examines

415 the possible influence of polarization of recorded ground motion on the angular difference
 416 between the orientation of maximum spectral response and the epicentral transverse

417 orientation for four oscillator periods subjected to both events in the Türkiye doublet.
 418 Scatterplot smoothing was performed starting at points from the ends where at least 1% of

419 the total data points are available. This is necessary since the smoothing is highly sensitive
 420 to the small number of data points at the tails that may not be representative of the trends

421 (i.e., this region is characterized by very wide confidence bands).



422

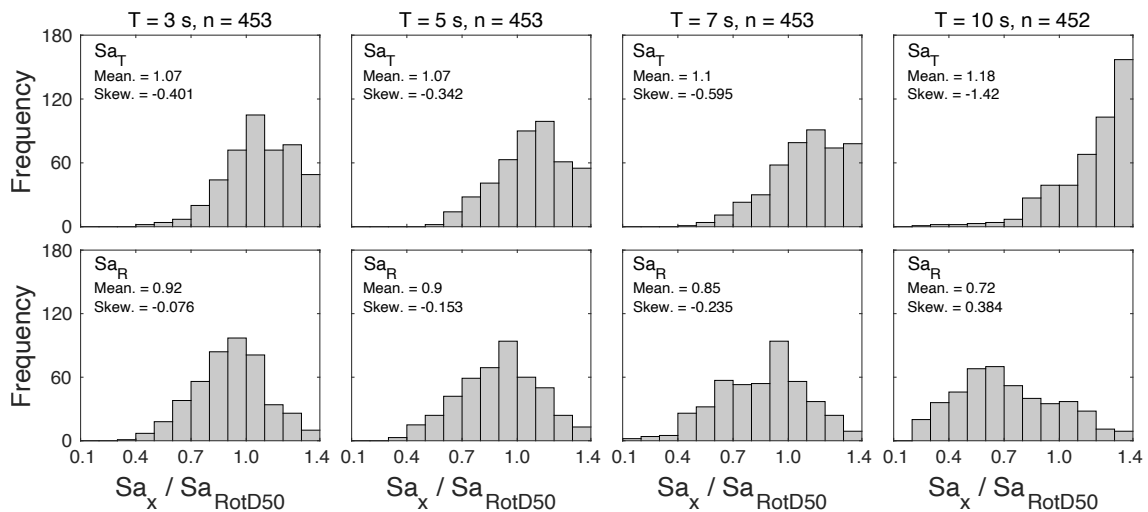
423 **Figure 10.** Evaluation of the possible influence of the level of polarization, as measured by
 424 RotD00/RotD100, on the angular difference between the epicentral transverse orientation and the
 425 orientation of RotD100 for periods of $T = 3$ s, $T = 5$ s, $T = 7$ s, and $T = 10$ s. The dashed line
 426 represents locally weighted scatterplot smoothing (LOWESS) considering both the M_w 7.8 and 7.5
 427 events. LOWESS was performed starting and ending at points where at least 1% of the data points
 428 are available.

429 As shown in Figure 10, the scatter points are generally clustered towards the bottom (i.e.,
 430 toward low values of $|\alpha|$). As the period of oscillator increases, the cluster in the bottom
 431 quadrant of the plots gets denser and shifts towards the left with more stations
 432 simultaneously exhibiting high polarization and an orientation of maximum intensity closer
 433 to the epicentral transverse orientation. Furthermore, the LOWESS for each period suggest
 434 that as the level of polarization decreases (i.e., RotD00/RotD100 increases), $|\alpha|$ tends to
 435 increase. This means that the epicentral transverse orientation may be good at estimating
 436 the orientation of maximum response for highly polarized motions but may not be as good
 437 for motions with small level of polarization. This observation is important because, if the
 438 motion is strongly polarized, it shows a clear orientation with strong intensity, and the
 439 estimation of this orientation becomes important. Meanwhile, if the motion is not strongly
 440 polarized, determining its orientation of maximum response is not as important.

441 SEISMIC INTENSITY AT TRANSVERSE AND RADIAL ORIENTATIONS

442 In the prior two sections, it has been shown that the orientation of maximum intensity for
 443 the Türkiye doublet tends to be close to the epicentral or maximum slip orientations,
 444 consistent with the findings of Poulos and Miranda (2023) for strike-slip earthquakes.

445 Awareness of the orientations where strong and weak spectral responses will occur could
 446 be beneficial in the development of orientation-dependent ground motion models. Most
 447 current ground motion models, including those used in the NGA-West2 project (e.g., Boore
 448 et al., 2014), predict only the median intensity (i.e., RotD50) of all orientations. However,
 449 engineering design standards in the U.S. use the maximum intensity (RotD100). If the
 450 intensity of the transverse orientation is used to estimate the maximum intensity, then it
 451 would be important to study the intensity at the transverse orientation relative to that of
 452 RotD50. This can be achieved by computing the ratio of the intensity at the transverse
 453 orientation to the RotD50 intensity (Sa_T/Sa_{RotD50}). This ratio can be used as a conversion
 454 factor to transform RotD50 intensities estimated using existing ground motion models to
 455 the intensity at the transverse orientation, which can then be used for engineering design.
 456 Figure 11 shows the distribution of the ratio between the spectral response at the transverse
 457 or radial orientation and RotD50 for four oscillator periods subjected to records obtained
 458 in the Türkiye doublet. Note that, at any orientation, the largest possible intensity is
 459 RotD100. Thus, the largest value any Sa_X/Sa_{RotD50} ratio can take is $\sqrt{2} = 1.41$.



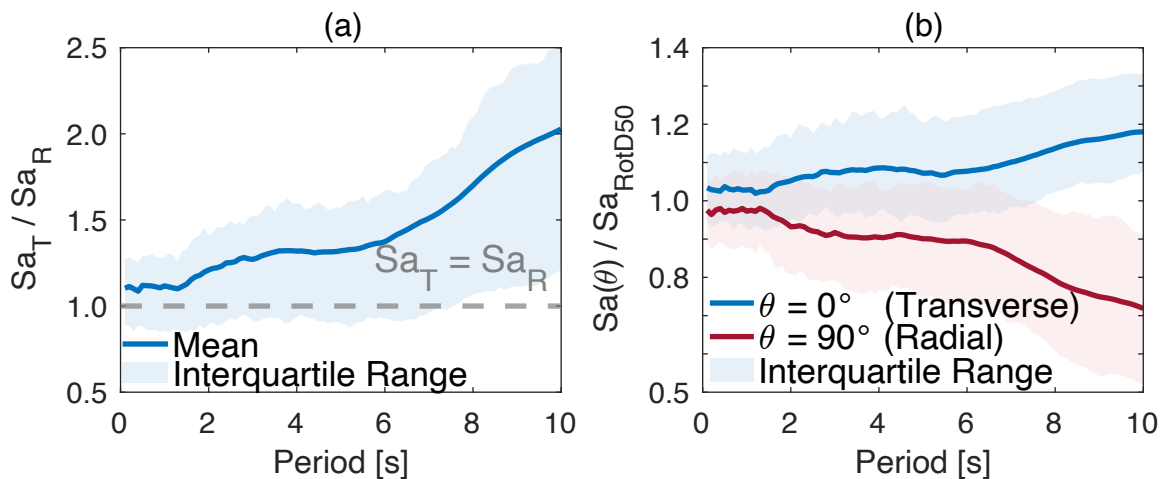
460

461 **Figure 11.** Histograms of the ratio between the ground motion intensity at the transverse or radial
 462 orientation and the median intensity (i.e., RotD50) for oscillators with fundamental periods of $T =$
 463 3 s, $T = 5$ s, $T = 7$ s, and $T = 10$ s. The sample size is indicated for each period and includes both
 464 the M_w 7.8 and 7.5 events in the sequence.

465 Multiple observations can be made from Figure 11. The intensity in the transverse
 466 orientation (top row) is notably larger than in the radial orientation (bottom row) at the four
 467 periods shown. Moreover, this difference in intensity between the transverse and radial
 468 orientations increases as oscillator period increases. This variation with oscillator period is
 469 further evaluated in Figure 12(a), where the mean intensity in the transverse orientation

470 increases nonlinearly from approximately 1.09 times the radial intensity at short periods to
 471 about two times the radial intensity for an oscillator of 10 s. Figure 11 also shows that the
 472 mean of $S_{aT}/S_{a_{RotD50}}$ shifts to the right and gets more skewed with increasing period. At a
 473 period of 10 s, more than 34% of the ratios are larger than 1.3. In contrast, the opposite
 474 trend is observed for $S_{aR}/S_{a_{RotD50}}$, with the mean shifting to the left with increasing period.
 475 Thus, the intensity at the transverse orientation is significantly above the median intensity
 476 of all orientations for most recording stations whilst the opposite holds for the radial
 477 orientation.

478 To better understand the influence of period, Figure 12(b) plots the variation in the mean
 479 $S_{aT}/S_{a_{RotD50}}$ ratio and $S_{aR}/S_{a_{RotD50}}$ ratio. The figure further illustrates the observations made
 480 in the histograms of these ratios for four periods. In particular, Figure 12(b) shows that
 481 mean $S_{aT}/S_{a_{RotD50}}$ ratios increase with period from approximately 1.02 at low periods to
 482 1.17 at 10 s. In contrast, mean $S_{aR}/S_{a_{RotD50}}$ ratios decrease at a more rapid rate from 0.98 at
 483 low periods to 0.73 at 10 s. Figure 11 and Figure 12 imply that, for this earthquake doublet,
 484 the mean intensity from all orientations in the epicentral transverse orientation
 485 systematically exceeds the median intensity for all oscillator periods, while intensities at
 486 the radial orientation are practically always lower than RotD50 at all periods of vibration.
 487 These $S_{aT}/S_{a_{RotD50}}$ ratios identified can be used to develop correction factors for GMMs to
 488 eliminate the systematic underestimation of ground motion intensities at the transverse
 489 orientation.



490

491 **Figure 12.** Influence of period of vibration on the mean ratio between (a) the intensity at the
 492 transverse orientation and the radial orientation and (b) the intensity at the transverse orientation or
 493 radial orientation and the RotD50 intensity. Shaded bands around the means indicate the
 494 interquartile range at each period.

495 **SUMMARY AND CONCLUSIONS**

496 The directionality of ground motions recorded during the February 6, 2023 M_w 7.8
497 Kahramanmaras and M_w 7.5 Elbistan earthquakes in the Türkiye doublet has been
498 investigated. The orientation of 5%-damped maximum spectral response and its spatial
499 distribution have been carefully studied. The spatial distribution of the level of polarization
500 and intensity at specific orientations were also investigated.

501 At present, the consensus for cases with no strong site effects is that at distances greater
502 than 5 km from the rupture, ground motions do not have a predominant orientation. In this
503 paper, it was found that the orientation of maximum response is systematically close to the
504 epicentral transverse orientation (i.e., orientation perpendicular to a line segment
505 connecting epicenter to station), consistent with previous observations by Poulos and
506 Miranda for other strike-slip earthquakes.

507 For the M_w 7.8 event, where the point of maximum slip was relatively far from the
508 epicenter, it was found that the orientation of maximum response is, on average, closer to
509 the orientation perpendicular to the maximum slip transverse orientation (i.e.,
510 perpendicular to a line connecting the station to the projection of the point of maximum
511 slip) when compared to the epicentral transverse orientation. This suggests that the
512 maximum slip transverse orientation may be a better estimator for orientation of maximum
513 response in large magnitude earthquakes where rupture size becomes important in the near
514 field, although further study using more events is warranted. Furthermore, the orientation
515 of maximum response was found to be close to the epicentral or maximum slip transverse
516 for Joyner-Boore distances up to 400 km, indicating that for strike-slip earthquakes there
517 is a predominant orientation even at long distance to the rupture. These findings further
518 support the case for the development of orientation-dependent ground motion models
519 where the orientation of maximum response is predicted by either the epicentral or
520 maximum slip transverse orientation.

521 Response of oscillators subjected to the M_w 7.8 Kahramanmaras and M_w 7.5 Elbistan
522 earthquakes were found to be fairly polarized at short periods and highly polarized at long
523 periods. Polarized motions were observed over large geographical areas and Joyner-Boore
524 distances up to 400 km. As ground motion records become more polarized, the orientation
525 of maximum intensity tends to be closer to the epicentral or maximum slip transverse.
526 Lastly, the intensity at the epicentral transverse orientation was on average 1.02 to 1.17

527 times larger than the median intensity from all orientations (RotD50) (depending on
528 period), indicating that current GMMs systematically underestimate the ground motion
529 intensity in the transverse orientation in strike-slip earthquakes. These types of results can
530 be used in the future to improve the estimation of the ground motion intensity at specific
531 orientations.

532 **ACKNOWLEDGMENTS**

533 The authors would like to thank the financial support they received that allowed them to
534 conduct this investigation. The first author received funding from the John A. Blume
535 fellowship from Stanford University. The second author received funding from the National
536 Agency for Research and Development (ANID) / Doctorado Becas Chile / 2019-72200307,
537 and from the Nancy Grant Chamberlain Fellowship from Stanford University. The authors
538 are also grateful to the Turkish Disaster and Emergency Management Authority (AFAD)
539 which operates the Turkish National Strong Motion Network for installing and maintaining
540 strong motion instrumentation in Türkiye and for collecting, processing, and distributing
541 the ground motions used in this study through their Turkish Accelerometric Database and
542 Analysis System (TADAS). The authors would also like to thank Dr. M. Abdullah
543 Sandikkaya and Dr. Sinan Akkar for the information they provided on the strong motion
544 recordings in the Türkiye earthquakes.

545 **REFERENCES**

- 546 Abrahamson NA and Silva WJ (1997) Empirical response spectral attenuation relations for shallow
547 crustal earthquakes. *Seismological Research Letters* 68(1): 94–127.
- 548 American Society of Civil Engineers (ASCE) (2016) *Minimum Design Loads for Buildings and*
549 *Other Structures, ASCE/SEI 7-16*. Reston, VA
- 550 American Society of Civil Engineers (ASCE) (2022) *Minimum Design Loads for Buildings and*
551 *Other Structures, ASCE/SEI 7-16*. Reston, VA
- 552 AFAD, Turkish Disaster and Emergency Management Presidency (AFAD) (2023a) 06.02.2023
553 01:17:32 Pazarcık (Kahramanmaraş) Earthquake MW 7.7. Available from:
554 <https://tadas.afad.gov.tr/event-detail/17966> (accessed April 2023).
- 555 AFAD, Turkish Disaster and Emergency Management Presidency (AFAD) (2023b) 06.02.2023
556 10:24:47 Elbistan (Kahramanmaraş) Earthquake MW 7.6. Available from:
557 <https://tadas.afad.gov.tr/event-detail/17969> (accessed April 2023).

558 Akkar S, Çağnan Z, Yenier E, et al. (2009) The recently compiled Turkish Strong Motion Database:
559 Preliminary Investigation for Seismological Parameters. *Journal of Seismology* 14(3): 457–479.

560 Ancheta, T. D., Darragh, R. B., Stewart, J. P., Seyhan, E., Silva, W. J., Chiou, B. S. J., ... & Donahue,
561 348 J. L. (2014) NGA-West2 database. *Earthquake Spectra*, 30(3): 989-1005.

562 Beyer K and Bommer JJ (2006) Relationships between median values and between aleatory
563 variabilities for different definitions of the horizontal component of motion. *Bulletin of the*
564 *Seismological Society of America* 96(4A): 1512–1522.

565 Boore DM (2010) Orientation-independent, nongeometric-mean measures of seismic intensity
566 from two horizontal components of motion. *Bulletin of the Seismological Society of America*
567 100(4): 1830–1835.

568 Boore DM, Joyner WB and Fumal TE (1997) Equations for estimating horizontal response spectra
569 and peak acceleration from Western North American earthquakes: A summary of recent work.
570 *Seismological Research Letters* 68(1): 128–153.

571 Boore DM, Watson-Lamprey J and Abrahamson N (2006) Orientation-independent measures of
572 ground motion. *Bulletin of the Seismological Society of America* 96(4A): 1502–1511.

573 Boore DM (2004) Choosing the Lowest Usable Frequency for Response Spectra from Filtered
574 Data. Available from:
575 http://www.daveboore.com/daves_notes/lowest_usable_freq_for_response_spectra_v20.pdf

576 Boore DM, Stewart JP, Seyhan E, et al. (2014) NGA-WEST2 equations for predicting PGA, PGV,
577 and 5% damped PSA for shallow crustal earthquakes. *Earthquake Spectra* 30(3): 1057–1085.

578 Boore DM and Kishida T (2017) Relations between some horizontal-component ground-motion
579 intensity measures used in practice. *Bulletin of the Seismological Society of America* 107(1): 334–
580 343.

581 Campbell KW and Bozorgnia Y (2008) NGA ground motion model for the geometric mean
582 horizontal component of PGA, PGV, PGD and 5% damped linear elastic response spectra for
583 periods ranging from 0.01 to 10 s. *Earthquake Spectra* 24(1): 139–171.

584 Earthquake Engineering Research Institute (EERI) and Geotechnical Extreme Event
585 Reconnaissance Association (GEER) (2023) *February 6, 2023 Türkiye Earthquakes: Report on*
586 *Geoscience and Engineering Impacts*, rep. Available from:
587 https://learningfromearthquakes.org/images/2023_02_06_nurdagi_turkey/GEER_2023_Turkey_Earthquake_FullReport_ReducedSize.pdf (accessed 7 May 2023).

588

589 Emre, Ö., Duman, T.Y., Özalp, S. *et al.* (2018). Active fault database of Turkey. *Bull. Earthquake*
590 *Eng.* **16**, 3229–3275.

591 Hong HP and Goda K (2007) Orientation-dependent ground-motion measure for seismic-hazard
592 assessment. *Bulletin of the Seismological Society of America* 97(5): 1525–1538.

593 Huang Y-N, Whittaker AS and Luco N (2008) Maximum spectral demands in the near-fault region.
594 *Earthquake Spectra* 24(1): 319–341.

595 Joyner WB and Boore DM (1982) Estimation of response-spectral values as functions of
596 magnitude, distance, and site conditions. *Open-File Report*.

597 Kullback S and Leibler RA (1951) On information and sufficiency. *The Annals of Mathematical*
598 *Statistics* 22(1): 79–86.

599 Mai PM, Spudich P and Boatwright J (2005) Hypocenter locations in finite-source rupture models.
600 *Bulletin of the Seismological Society of America* 95(3): 965–980.

601 NEHRP Consultants Joint Venture (2011). *Selecting and Scaling Earthquake Ground Motions for*
602 *Performing Response-History Analysis, Tech. Rep. NIST GCR 11-917-15*, Washington, D.C.

603 Paolucci R, Pacor F, Puglia R, G. Ameri, C. Cauzzi, and M. Massa (2011) Record processing in
604 Itaca, the new Italian strong-motion database. *Earthquake Data in Engineering Seismology*: 99–
605 113.

606 Poulos A and Miranda E (2022) Probabilistic characterization of the directionality of horizontal
607 earthquake response spectra. *Earthquake Engineering & Structural Dynamics* 51(9): 2077–2090.

608 Poulos, A. and Miranda, E. (2023) ‘Effect of style of faulting on the orientation of maximum
609 horizontal earthquake response spectra’, *Bulletin of the Seismological Society of America*
610 [Preprint]. doi:10.1785/0120230001.

611 Shahi SK and Baker JW (2014) NGA-West2 models for ground motion directionality. *Earthquake*
612 *Spectra* 30(3): 1285–1300.

613 Somerville PG, Smith NF, Graves RW, et al. (1997) Modification of empirical strong ground motion
614 attenuation relations to include the amplitude and duration effects of rupture directivity.
615 *Seismological Research Letters* 68(1): 199–222.

616 United States Geological Survey (USGS) (2023a). M 7.8 - Pazarcik earthquake, Kahramanmaras
617 earthquake sequence. Event Page. Available from:
618 <https://earthquake.usgs.gov/earthquakes/eventpage/us6000jllz/executive> (accessed 13 April 2023).

619 United States Geological Survey (USGS) (2023b). M 7.5 – Elbistan earthquake, Kahramanmaras
620 earthquake sequence. Event Page. Available from:
621 <https://earthquake.usgs.gov/earthquakes/eventpage/us6000jlqa/executive> (accessed 13 April 2023).